LOW DIMENSIONAL MANIFOLD EMBEDDING FOR SCATTERING COEFFICIENTS OF INTRAPARTUM FETALE HEART RATE VARIABILITY

V. Chudacek[1,5], R. Talmon[2], J. Anden[3], S. Mallat[3], R. R. Coifman[2], P. Abry[1], M. Doret[4]

Abstract— **Intrapartum fetal surveillance for early detection of fetal acidosis in clinical practice focuses on reducing neonatal morbidity via early detection. It is the subject of on going research studies attempting notably to improve detection performance by reducing false positive rate. In that context, the present contribution tailors to fetal heart rate variability analysis a graph-based dimensionality reduction procedure performed on scattering coefficients. Applied to a high quality and well-documented database constituted by obstetricians from a French academic hospital, the low dimensional embedding enables to distinguish between the temporal dynamics of healthy and acidotic fetuses, as well as to achieve satisfactory detection performance detection compared to those obtained by the clinical-benchmark FIGO criteria.**

Index Terms— **Intrapartum fetal heart rate variability, Scattering transform, Dimensionality reduction, Embedding,**

I. Motivation, goals and contributions

Intrapartum Fetal Heart Variability surveillance. Monitoring intrapartum fetal heart rate is a routine clinical procedure that aims notably at detecting fetal acidosis as early as possible. Early detection enables obstetricians to perform operative deliveries whenever necessary and thus to reduce fetal and neonatal mortality and morbidity due to asphyxia [1]. The health status of the fetus is essentially assessed by analysis of the fetal heart rate variability (F-HRV), i.e., the fluctuations of the RR-interval times.

Related work. F-HRV analysis often relies on two different steps: i) Extraction of features, discriminating the temporal dynamics of healthy fetuses from that of fetuses suffering from acidosis ; ii) Application of a supervised or unsupervised classification procedure to assess the fetus health status. For the first step, at the clinical level, F-HRV analysis relies on the FIGO criteria [2], which mostly comprise morphological or geometrical features (e.g., depths or widths of decelerations) or statistical time domain features (e.g., long term or short term variabilities, cf. e.g., [3]). At the research level, spectral domain features have been massively used to characterize F-HRV temporal dynamics and thus to detect fetuses suffering from acidosis (cf. [4], [5] for reviews). Dynamical system oriented analysis tools have also been used, amongst which entropy rates [6] and other non linear analysis methods, which exploit information beyond linear correlation (cf. [4], [7]). Recently, the concepts of self-similarity and its non linear extension, multifractal analysis, have also been used in that context (cf. e.g., [4], [8], [9]). The second step often consists in feeding nowadays standard yet advanced supervised classifiers (such as Support Vector Machines, SVM) with usually large sets of features (cf. e.g, [10]). Such practices are driven by the underlying expectation that the elaborated classification procedure will make the best of the high dimensional representation stemming from the large collection of features, each carrying individually only a weak classification power.

Goals and contributions. The present contribution aims at showing that F-HRV time series, despite resulting from complex physiological mechanisms, which can be viewed as complex dynamical systems, can be well represented by a low-dimensional dynamical system that captures essential information relevant for intrapartum surveillance. This representation relies on a new signal processing algorithm, which approximates a dynamical system by constructing a low-dimensional manifold embedding of scattering coefficients. Scattering transforms were shown to well preserve information crucial for acidosis detection [11]. The scattering transform is introduced in Section III, while the graph-based algorithm permitting the low dimensional embedding of data is described in Section IV. It is applied to a high quality F-HRV database constituted at the academic Hospital *Femme-mère-Enfant* (HFME, Women-Mother-Child Hospital) in Lyon, France (cf. Section II). Results are reported in Section V and show that the variability of F-HRV scattering coefficients, computed within two-minute sliding window, is well captured by a low-dimensional manifold, and that dimensionality reduction enables us to use a *simple* nearest neighbor procedure as an effective classifier for acidosis detection. Combined with obstetrician's annotations, the achieved detection sheds new and interesting light on acidotic and healthy fetus temporal dynamics and on the reasons why particular cases are difficult to classify.

II. Database

Data measurements. At HFME, Fetal heart rate surveillance and recordings is clinically performed using the STAN, Neoventa Medical (Moelndal, Sweden) system (STAN 21 or 31 systems, 12bit resolution, which produces high quality F-

Work supported by ANR BLANC 2010 FETUSES 18535, HCL-HFME PHRC, ANR-10-BLAN-0126, ERC InvariantClass 320959, Czech Grant Agency, 14-28462P.

[1] Physics Dept. - ENSL, CNRS UMR 5672, Lyon, France, patrice.abry@ens-lyon.fr
[2]Math. Dept. - Yale University, USA, ronen.talmon@yale.edu
[3] Math Dept. - ENS, CNRS, Paris, France, mallat@cmap.polytechnique.fr, joakim.anden@gmail.com
[4] Femme-Mère-Enfant Hospital, Lyon, France, muriel.doret@chu-lyon.fr
[5] Czech Technical University, Prague

HRV recording, with low level of missing data and corrupted signals. From electrocardiograms, lists $\{t_n\}_{n\in\mathbb{N}}$, of beat-by-beat R-peak occurrence times (in ms) are extracted and made available for analysis.

Database. Obstetricians at HFME have created a database of intrapartum F-HRV data, representative of healthy subjects and of fetuses suffering from acidosis, and organized it into three classes (cf. [8] for detailed description): i) **FIGO-TP:** 15 fetuses suffering from fetal acidosis, with post birth measured arterial umbilical cord umbilical pH ≤ 7.05, hence abnormal, which were correctly diagnosed as such according to FIGO-guidelines, and thus referred to as FIGO-True Positives ; ii) **FIGO-TN:** 15 non acidotic (healthy) fetuses, i.e., with normal fetal outcome, and post birth measured arterial umbilical cord pH ≥ 7.30, which were correctly diagnosed as such according to FIGO-guidelines, and thus referred to as FIGO-True Negatives ; iii) **FIGO-FP:** 15 fetuses non acidotic (healthy) fetuses, i.e., with normal fetal outcome, with post birth measured arterial umbilical cord pH ≥ 7.30, which were yet incorrectly diagnosed as acidotic according to FIGO-guidelines, and thus referred to as FIGO-False Positives. All recording last for more than 30 minutes.

The database is also *documented* by obstetricians, notably with annotations motivating decisions for diagnosis and operative delivery. One issue obstetricians are struggling with is the high level of false positive detections, which stems from the very nature of the application: Misdetection of fetuses suffering from acidosis during the delivery process would yield dramatic consequences; FIGO-guidelines are thus defined stringently so as to avoid such misdetections (False Negatives), at the expense, though, of a high False Positive rate. A diagnostic that the fetus suffers from a precursory acidosis often leads to an operative delivery decision (C-section, ...), which may also, in a number of cases, induce undesirable post birth complications, for both the mother and the newborn. Reducing the False Positive rate has thus attracted significant and continuous research efforts, at both the clinical and academic levels, a goal to which the present work contributes.

From the current database, FIGO-criteria provide us with reference and benchmark detection performance: Sensitivity of $100\% = TP/(TP+FN)$, at the price of Specificity of $50\% = FP/(TP+FP)$, a Matthews correlation coefficient (MCC) [13] of 50% and an overall miss-classification (or Error) rate of $33\% = (FP+FN)/(TP+TN+FP+FN)$ (cf. Table I, line 1).

Preprocessing. Often in F-HRV analysis (cf. e.g., [4], [5]), the series of R-Peak occurrences $\{t_n\}_{n\in\mathbb{N}}$ are transformed, prior to analysis, into regularly sampled Beat-per-Minute (BpM) time series, by interpolation of the samples $\{(t_n/1000, 60000/(t_{n+1}-t_n))\}_n$. The chosen sampling frequency is here $f_s = 8$ Hz, as F-HRV does not convey any physiological information beyond 3 Hz.

III. Scattering transform

It is now well-accepted that F-HRV signals are characterized by stationary multiscale temporal dynamics, within time scales ranging from seconds to minutes (cf. e.g., [4], [8], [9]) . Scattering coefficients provide stable characterizations for such processes, by iteratively applying a wavelet transform to the modulus of complex wavelet coefficients [14]. Scattering coefficients have been proven useful for many different applications and notably for capturing essential information for acidosis detection [11].

Let $X(t)$ denote the time series to analyze and let $\psi(t)$ denote a complex analytic mother wavelet (thus band-pass filter). Let $\psi_j(t) = 2^{-j}\psi(2^{-j}t)$ denote the collection of dilated templates of ψ at scales 2^j. Also, let $\phi(t)$ denote the scaling function (thus low pass-filter), associated with the mother wavelet $\psi(t)$. The first order scattering coefficients are defined as the average amplitude of the modulus of the wavelet coefficients $X \star \psi_j(t)$, for any $1 \leq j \leq J$, over 50% overlapping time windows of size 2^J, centered at time positions $t = k2^{J-1}$, $k \in \mathbb{N}$:

$$SX(j,k) = |X \star \psi_j| \star \phi_J(t = k2^{J-1}) \ . \tag{1}$$

The convolution with the low-pass filter ϕ_J performs an averaging over a time interval of size 2^J. However, this averaging loses information on the time variability of $|X \star \psi_j(t)|$. This information is recovered by computing a second set of wavelet coefficients $|X \star \psi_{j_1}(t)| \star \psi_{j_2}(t)$. Second order scattering coefficients are defined, at each $t = k2^{J-1}$, for any $1 \leq j_1 < j_2 \leq J$, as:

$$SX(j_1,j_2,k) = ||X \star \psi_{j_1}| \star \psi_{j_2}| \star \phi_J(t = k2^{J-1}) \ . \tag{2}$$

Higher order scattering coefficients are defined by repeating this procedure. For example, third order coefficients are defined for any $1 \leq j_1 < j_2 < j_3 \leq J$ by $SX(j_1,j_2,j_3,t) = |||X \star \psi_{j_1}| \star \psi_{j_2}| \star \psi_{j_3}| \star \phi_J(t)$. Here, we concentrate on scattering coefficients of order one and two which gather most of the energy of the process. Because the amplitude of second order scattering coefficients is proportional to that of the first order coefficients, the former are renormalized by the latter:

$$\widetilde{S}X(j_1,j_2,k) = \frac{SX(j_1,j_2,k)}{SX(j_1,k)} \ . \tag{3}$$

The vector of scattering coefficients (of size $N = J + J \times (J-1)/2 - 1$) is defined as the logarithm of the first and normalized second order coefficients, for time k: $\mathcal{S}X(k) =$

$$\left(\{\log SX(j,k)\}_{1\leq j\leq J} \ , \ \{\log \widetilde{S}X(j_1,j_2,k)\}_{1\leq j_1<j_2\leq J}\right) . \tag{4}$$

A Battle-Lemarié complex cubic spline wavelet [14] is used here. The ScatNet software is available at http://www.di.ens.fr/data/software/scatnet/.

IV. Low dimensional manifold embedding

The scattering coefficients $\mathcal{S}X(k)$ are viewed as points in a high N-dimensional space. Assuming that the data is governed by merely few physiological factors implies that $\mathcal{S}X(k)$ do not fill the high dimensional space uniformly, but rather, lie in a low dimensional manifold. The investigation of the existence of such a low dimensional structure has recently

become common practice in a broad range of applications relying on various different techniques (cf. e.g. [15] and reference therein). In the present work, a particular manifold learning method, especially designed to exploit temporal dynamics, is applied [12].

The local variability of the high dimensional data, as captured through the covariance of the vectors in short time windows, is used to define a Riemannian metric. Let $\mathbf{C}(k)$ denote the covariance matrix of $\mathcal{S}X(k)$ and $\widehat{\mathbf{C}}(k)$ its estimate in short windows of length $2L+1$ centered at time frame k:

$$\widehat{\mathbf{C}}(k) = \sum_{l=k-L}^{k+L} (\mathcal{S}X(l) - \widehat{\boldsymbol{\mu}}(k))^T (\mathcal{S}X(l) - \widehat{\boldsymbol{\mu}}(k)) \qquad (5)$$

where $\widehat{\boldsymbol{\mu}}(k)$ is the empirical mean of the vectors in the window. Let D denote the dimension of the manifold, where usually $D \ll N$. Since the variations of the data in N dimensions are confined to a D dimensional structure, the rank of the local covariance matrices of size $N \times N$ is D, with twofold consequences: First, the empirical ranks of the covariance matrices estimate the dimension of the manifold. Second, assuming this dimension is fixed, the consistency of the rank over time indicates that sufficient data is available.

Scattering coefficients are obtained from time-averaging, and have been shown to have a nearly Gaussian distribution. For Gaussian random vectors, log probabilities are defined by the Mahalanobis distance, yielding Riemannian metric between pairs of vectors of scattering coefficients:

$$d(k,l) = (\mathcal{S}X(k) - \mathcal{S}X(l))^T (\mathbf{C}(k) + \mathbf{C}(l))^{-1} (\mathcal{S}X(k) - \mathcal{S}X(l)) \qquad (6)$$

The Mahalanobis distance is invariant to local affine distortions, and has recently been used to better reveal the governing states of dynamical systems [16], [17], [12].

This Mahalanobis distance is further used to construct a $K \times K$ kernel matrix $\mathbf{W}$ consisting of pairwise affinities between vectors, with ε a tunable kernel scale and K the number of available time frames:

$$W_{kl} = \exp\left\{-\frac{d(l,k)}{\varepsilon}\right\}, \quad k,l = 1,\ldots,K. \qquad (7)$$

The kernel defines a weighted graph, where nodes $\mathcal{S}X(k)$ and $\mathcal{S}X(l)$ are connected by an edge with weight W_{kl}. Thus, each vector is effectively connected to other vectors that are within ε vicinity with respect to the Mahalanobis distance (6). Let $\mathbf{D}$ be a diagonal $K \times K$ matrix, whose diagonal elements are given by $D_{kk} = \sum_l W_{kl}$, and let $\mathbf{W}^{\text{norm}} = \mathbf{D}^{-1/2}\mathbf{W}\mathbf{D}^{-1/2}$ be a normalized kernel that shares its eigenvectors with the normalized graph-Laplacian $\mathbf{I} - \mathbf{W}^{\text{norm}}$ [18].

Applying the eigenvalue decomposition (EVD) to $\mathbf{W}^{\text{norm}}$ yields a set of eigenvalues and eigenvectors, denoted by λ_i and $\boldsymbol{\nu}_i$, respectively. A nonlinear embedding of the vectors $\mathcal{S}X$ into a D dimensional space is constructed:

$$\mathcal{S}X(k) \mapsto (\nu_1(k), \nu_2(k), \ldots, \nu_D(k)). \qquad (8)$$

While the kernel represents local connections, a global representation that is traditionally viewed as the parameterization of the manifold is obtained through the eigenvectors of the kernel that implicitly integrates the local connections.

V. Fetal Heart Rate Variability Embedding

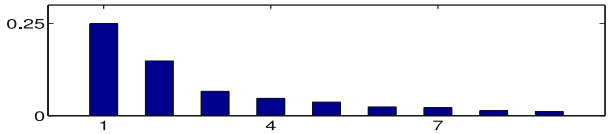

Fig. 1. **Decay of sorted embedding eigenvalues.**

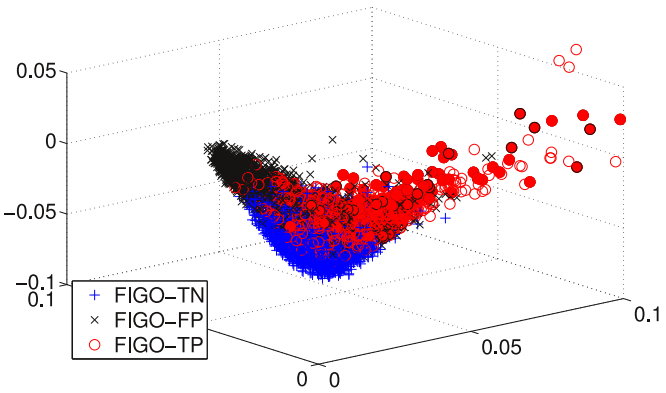

Fig. 2. **Low-Dimensional Manifold Time-Window Embedding.** Each time-window of each subject is mapped into the 3D coordinates of the embedding space. Blue '+' correspond to FIGO-TN (healthy) subjects, black 'x' to FIGO-FP (healthy) subjects and red 'o' to FIGO-FP (acidotic) subjects Amongst FIGO-FP, filled red circles correspond to time windows at most 6 minutes before delivery.

Scattering coefficients. To study the time evolution (or trajectories) of the temporal dynamics of F-HRV BpM time series and thus of the fetus health status, scattering coefficients $\mathcal{S}X(k)$ (cf. Eq. 4) are computed, for each subject, across the entire F-HRV time series, within sliding windows of size $\simeq$ 2min, with 50% overlap, with $J = 10$, yielding $2^J/f_s = 128$s. Parameter $J = 10$ is chosen such because it is known from previous works (cf. e.g., [4], [5], [8]) that F-HRV temporal dynamics relevant to acidosis detection involve time scales ranging from 1s to 1min. The choice of a 2min-long window the computation of the $\mathcal{S}X(k)$ (cf.Eq. 4) yields empirically maximal classification performance and is consistent with the physiological information dynamics ranging from seconds to minutes. For each time window, $\mathcal{S}X(k)$ has dimension $N = 55$.

Embedding procedure. The embedding procedure is applied to the collection of the $\mathcal{S}X(k)$ computed along the entire trajectories for $P = 45$ (subjects), resulting into $K = 5952$ time positions. Embedding parameters ϵ and L (cf. Section IV) are selected empirically by checking a posteriori that the eigenvalues λ_i of $\mathbf{W}^{\text{norm}}$ exhibit a smooth decay (as shown in Fig. 1), and set to $\epsilon = 30$ and $L = 10$.

Low-dimensional manifold embedding. Fig. 2 displays the mapping of each time-window for each subject into the embedding space, restricted to its 3 first dimensions (setting $D = 3$). It clearly illustrates that the data create a *croissant*-shaped low dimensional manifold, showing a number of interesting features. First, the three classes are spread along

a continuum on the manifold, yet tend to concentrate in different sub-parts of the manifold. Second, acidotic fetuses (FIGO-TP) clearly depart from healthy subjects (FIGO-FP and FIGO-TN). Third, amongst Healthy subjects, the FIGO-FP do form a different cluster from the FIGO-TN, yet this cluster departs *to the left* from the FIGO-TN cluster,while the FIGO-TP cluster departs *to the right*. This result exemplifies and explains the difficulty in this classification problem.

	Sensitivity	Specificity	MCC	Error-rate
FIGO	100 (–)	50 (–)	50 (–)	33 (–)
Emb+NN	66 (29)	89 (15)	62 (29)	18 (13)
SVM	60 (27)	93 (10)	59 (26)	18 (10)

TABLE I

Classification Performance in %. MEAN (STD) OBTAINED FROM AVERAGE ON 100 REPETITIONS OF THE CLASSIFICATION PROCEDURES. MCC STANDS FOR MATTHEWS CORRELATION COEFFICIENT [13].

Classification performance. To quantify the embedding quality, a *Nearest Neighbor* classifier procedure, which is asymptotically optimal when data density increases, is implemented on the manifold (referred to as Emb+NN). It is compared against a (Gaussian Kernel-based) SVM classifier (cf. e.g., [19]), applied directly to vectors of scattering coefficients $\mathcal{S}X(k)$, which does not rely on any dimensionality reduction. For both procedures, training and testing sets contain 80% and 20% of the available subjects respectively. The last 16 time-windows (corresponding roughly to 17min before delivery) of each subject are used as input. For each subject in the testing set, the time-windows are classified independently, and the status (Healthy or UnHealthy) of a given subject is selected by majority voting. The parameters of both procedures (kernel width and slackness parameter for SVM, dimension D and number of nearest neighbors) are optimized during training through five-fold cross-validation. This is repeated 100 times for different train-test partitions to compute average classification performance, with means and standard deviations reported in Table I. The *advanced* SVM classifier usually provides better results than the *simple* nearest neighbor procedure. Table I shows that here Nearest Neighbors performed on the low dimensional manifold (Line 2) achieves performance comparable to that of SVM (Line 3). This constitutes a clear validation that the dimensionality embedding captures most of the relevant temporal dynamics involved in acidosis detection.

Classification analysis. In Fig. 2, it can be seen that several FIGO-FP subjects fall into the FIGO-TP embedding domain, while others fall into the FIGO-TN embedding domain. Making use of obstetrician annotations allows to identify that the former group consists of subjects showing *complicated-shape* and *severe* decelerations, while the latter group consists of subjects showing *Low-Variability* or *Low-reactivity*. Such low dimensional representations thus yield interesting analysis of the temporal dynamics of healthy and acidotic fetuses: FIGO-TP acidotic trajectories and temporal dynamics clearly differ from those of FIGO-TN healthy subjects ; FIGO-FP subjects showing severe decelerations have temporal dynamics that very much resemble that of acidotic subjects and thus cannot be easily discriminated from them ; FIGO-FP subjects showing low-variability and/or low reactivity have temporal dynamics that may differ from those of FIGO-TN subjects yet that also depart from that of acidotic fetuses and can thus be distinguished from them.

VI. CONCLUSIONS AND PERSPECTIVES

A graph based dimensionality reduction methods applied to the scattering coefficients of F-HRV time series yields new and fruitful analyses of differences between the temporal dynamics of healthy and acidotic fetuses, as well as acidosis detection performance that outperforms those obtained with the benchmark FIGO criteria. Application to a larger database is under current investigation.

REFERENCES

[1] I. Amer-Wahlin et al., "Cardiotochography only versus cardiotochography plus st analysis of fetal electrocardiogram for intrapartum fetal monitoring: a swedish randomised controlled," *Lancet.*, vol. 358, no. 9281, pp. 534–538, 2001.

[2] FIGO, "Guidelines for the use of fetal monitoring," *Int. J. Gynaecol. Obstet.*, vol. 25, pp. 159–167, 1987.

[3] J. Bernardes and D. Ayres-De-Campos, "The persistent challenge of fetal heart rate monitoring," *Current Opinion in Obstetrics and Gynecology*, vol. 22, no. 2, pp. 104–109, 2010.

[4] P. Hopkins et al., "A comparative study of fetal heart rate variability analysis techniques," in *Proc. of the 28th IEEE EMBS Conf.*, 2006, pp. 1784–1787.

[5] J. Van Laar et al., "Spectral analysis of the fetal heart rate variability for fetal surveillance: review of the literature," *Acta Obstetrica et Gynecologica*, vol. 87, pp. 300–306, 2008.

[6] M. Cost et al., "Multiscale entropy analysis of biological signals," *Phys Rev E Stat Nonlin Soft Matter Phys*, vol. 71, no. 2 Pt 1, pp. 021906, Feb 2005.

[7] M. Ferrario et al., "Comparison of entropy-based regularity estimators: application to the fetal heart rate signal for the identification of fetal distress," *IEEE Trans. Biomed. Eng.*, vol. 53, no. 1, pp. 119–125, 2006.

[8] M. Doret et al., "Multifractal analysis of fetal heart rate variability in fetuses with and without severe acidosis during labor," *Am. J. Perinatol.*, vol. 28, no. 4, pp. 259–266, 2011.

[9] P. Abry et al., "Hurst exponent and intrapartum fetal heart rate: Impact of decelerations," in *The 26th IEEE International Symposium on Computer-Based Medical Systems*, 2013.

[10] G. Georgoulas et al., "Predicting the risk of metabolic acidosis for newborns based on fetal heart rate signal classification using support vector machines," *IEEE Trans. Biomed. Eng.*, vol. 53, no. 5, pp. 875–884, May 2006.

[11] V Chudáček et al., "Scattering transform for intrapartum fetal heart rate characterization and acidosis detection," in *35th Annual International Conference of the IEEE EMBS*, 2013, pp. 2898–2901.

[12] R. Talmon and R. Coifman, "Intrinsic modeling of stochastic dynamical systems using empirical geometry," *Submitted, Tech. Report YALEU/DCS/TR1467, 2013*,

[13] B.W. Matthews, "Comparison of the predicted and observed secondary structure of T4 phage lysozyme," *Biochim. Biophys. Acta*, vol. 405, pp. 442–451, 1975.

[14] S. Mallat, "Group invariant scattering," *Pure and Applied Mathematics*, vol. 10, no. 65, pp. 1331–1398, 2012.

[15] R. Coifman and S. Lafon, "Diffusion maps," *Appl. Comput. Harmon. Anal.*, vol. 21, pp. 5–30, Jul. 2006.

[16] A. Singer and R. Coifman, "Non-linear independent component analysis with diffusion maps," *Appl. Comput. Harmon. Anal.*, vol. 25, pp. 226–239, 2008.

[17] R. Talmon and R.R. Coifman, "Empirical intrinsic geometry for nonlinear modeling and time series filtering," *Proc. Nat. Acad. Sci.*, vol. 110, no. 31, pp. 12535–12540, 2013.

[18] F. R. K. Chung, *Spectral Graph Theory*, CBMS-AMS, 1997.

[19] C. Cortes and V. Vapnik, "Support-vector networks," *Machine learning*, vol. 20, no. 3, pp. 273–297, 1995.